Electronic Supplementary Material (ESI) for Dalton Transactions

Electronic Supplementary Information

$\{Co^{III}_2Dy^{III}_2\}$ single molecule magnet with two resolved thermal activated magnetization relaxation pathways at zero field

Alejandro V. Funes[a], Luca Carrella[b], Eva Rentschler[b] and Pablo Alborés[a]*.

[a]Departamento de Química Inorgánica, Analítica y Química Física/ INQUIMAE (CONICET), Facultad de Ciencias Exactas y Naturales Universidad de Buenos Aires, Pabellón 2, Ciudad Universitaria, C1428EHA Buenos Aires, Argentina. [b] Institute of Inorganic and Analytical Chemistry, Johannes Gutenberg - University of Mainz, Duesbergweg 10-14 D-55128 Mainz-Germany.

Experimental details.

[$Co_2(\mu\text{-}OH_2)(\mu\text{-}Piv)_2(Piv)_2(HPiv)_4$], Piv=trimethylacetate, was prepared following a previously reported procedure[1]. $Dy(NO_3)_3.xH_2O$ was prepared by reaction of $Dy_2O_3$with nitric acid in water. All other chemicals were reagent grade and used as receive without further purification. Elemental analysis for C, H and N were performed with a Carlo Erba 1108 analyzer.

Synthesis of $Dy_2Co_2(OMe)_2(teaH)_2(Piv)_6$ (1)

$Co_2(OH_2)(Piv)_4(HPiv)_4$ (100 mg, 0.1 mmol) and $Dy(NO_3)_3.xH_2O$ (68 mg, ~0.1 mmol) were dissolved in 10 mL of MeCN, followed by the addition of a triethanolamine (60 mg, 0.4 mmol) and triethylamine (61 mg, 0.6 mmol) dissolved in 10 ml of acetonitrile; affording a purple solution. The latter was then stirred for an hour, filtered and allowed to stand sealed at room temperature. Within 3-4 weeks a crop of blue needles appeared. This product was filtrated and re-dissolved in a MeCN/MeOH 1:1 mixture. After a couple of days blue blocks of **1** had crystallized in approximate yield of 25 % (26 mg). Anal. Calculated (found) for $C_{44}H_{86}Co_2Dy_2N_2O_{20}$ C, 37.6 (37.2); H, 6.2 (5.5); N, 2.0 (2.1).

Magnetic measurements: Magnetic measurements were performed with a Quantum Design MPMS XL-7 SQUID magnetometer. All experimental magnetic data were corrected for the diamagnetism of the sample holders and of the constituent atoms (Pascal's tables). DC measurements were conducted from 2 to 300 K at 1 kOe and between 2-10 K in the range 1-70 kOe. AC measurements were performed at driving frequencies ranging 10 to 1400 Hz with AC field amplitude of 3 Oe in zero DC field. In the samples where free movement of crystallites was prevented, silicone grease was employed for the embedding. When silicone is not used, sample completely aligned with field quantization axis as evidenced by the magnetization saturation values achieved.

X-ray Structure Determination: Crystal structure of compound **1** was determined with an Oxford Xcalibur, Eos, Gemini CCD area-detector diffractometer using graphite-monochromated Mo-*K*α radiation (λ = 0.71069 Å) at 298 K. Data was corrected for absorption with CrysAlisPro, Oxford Diffraction Ltd.,Version 1.171.33.66, applying an empirical absorption correction using spherical harmonics, implemented in SCALE3

ABSPACK scaling algorithm[2]. The structure was solved by direct methods with SHELXS-97[3] and refined by full-matrix least-squares on F^2 with SHELXL-97[3]. Hydrogen atoms were added geometrically and refined as riding atoms with a uniform value of U_{iso}. One of pivalate methyl groups was disordered around two positions and was refined with 0.5:0.5 occupancy factors. Final crystallographic data and values of R_1 and wR are listed in Table ESI1 while the main angles and distances are listed in Table ESI2.

Magnetic data analysis details.

In order to extract information from the DC susceptibility and magnetization experimental data, we attempted a full fitting by obtaining the energy of the exchange coupled lowest energy J=15/2 spin-orbit coupled states of Dy^{III} ion ($^6H_{15/2}$, S = 5/2, L = 5, J = 15/2, g_J=4/3) and calculating the molar magnetization and susceptibility with Eq. 1a and 1b for all possible field orientations:

$$M = \frac{N\sum_n \left(-\partial E_i/\partial H\right)\exp\left(-E_i/kT\right)}{\sum_i \exp(-E_i/kT)} \qquad (1a)$$

$$\chi_m = \frac{M}{H} \qquad (1b)$$

The energy of the different levels is obtained through diagonalization of the suitable Hamiltonian. In this case:

$$\hat{H} = g_J \beta H(\hat{J}_1 + \hat{J}_2) + B_0^2\left(\hat{O}_{10}^{\ 2} + \hat{O}_{20}^{\ 2}\right) + B_0^4\left(\hat{O}_{10}^{\ 4} + \hat{O}_{20}^{\ 4}\right) - 2J_{exc}\hat{S}_1\hat{S}_2 \qquad (2)$$

where the first term is the Zeeman component, the second and third terms are the crystal field component expressed as Steven's equivalent operators and the last one is the HDVV exchange interaction component. This Hamiltonian applies to the basis set: $\left|J_1 J_2 m_{J1} m_{J2}\right\rangle$, with J_1=J_2=15/2, L=5, S=5/2.

In the case of magnetization data fitting with a model based on an effective S_{eff}=1/2, the same procedure was applied with the following Hamiltonian:

$$\hat{H} = \beta(g_x^{eff}.\hat{S}_x^{eff}.H_x + g_y^{eff}.\hat{S}_y^{eff}.H_y + g_z^{eff}.\hat{S}_z^{eff}.H_z) \quad (3)$$

In a similar way, the alternative fitting of low temperature susceptibility data was carried out with an Ising Hamiltonian for two interacting S_{eff} doublets:

$$\hat{H} = -2J_z^{eff}\hat{S}_{1z}^{eff}\hat{S}_{2z}^{eff} + \beta g_z^{eff}\left(\hat{S}_{1z}^{eff} + \hat{S}_{2z}^{eff}\right)H \quad (4)$$

All Hamiltonian diagonalizations and fittings were performed employing the Easyspin 4.5.3[1] package together with home-made programmed routines.

Cole-Cole data was fitted employing a generalized Debye model including two different relaxation characteristic times:

$$\chi_{AC}(\omega) = \chi_{S,tot} + \frac{\Delta\chi_1}{1+(i\omega\tau_1)^{(1-\alpha_1)}} + \frac{\Delta\chi_2}{1+(i\omega\tau_2)^{(1-\alpha_2)}}$$

$$\chi_{S,tot} = \chi_{S1} + \chi_{S2} \qquad \Delta\chi_{1,2} = \chi_{T1,2} - \chi_{S1,2}$$

(1) S. Stoll, A. Schweiger; *J. Magn. Reson*. 2006, **178**(1), 42.

Low temperature magnetization relaxation dynamic behaviour analysis of previous reported {$Co^{III}_2Dy^{III}_2$} complexes.

The $[Co^{III}_2Dy^{III}_2(OR)_2(teaH)_2\ (acac)_4(NO_3)_2]$ complexes, show thermal barriers in the range 30-40 K, with QT characteristic times in the range 2-6 ms, reaching pure QT regimes at low temperature. These data can be nicely reproduced in the whole temperature range, with thermal barriers in agreement with the reported ones, (fig. S7) employing the law:

$$\frac{1}{\tau} = \frac{1}{\tau_0}\exp\left(-\frac{U_{eff}}{kT}\right) + \frac{1}{\tau_{QT}}$$

On the other hand, for the mixed crystal $[Co^{III}_2Dy^{III}_2(OMe)_2(teaH)_2(O_2CPh)_4(MeOH)_2][NO_3]_2$.

$[Co^{III}_2Dy^{III}_2(OMe)_2(teaH)_2(O_2CPh)_4(MeOH)_2(NO_3)_2]$ a thermal barrier of 89K was reported. However, when inspecting the ln(τ) vs 1/T data plot profile of this compound, it seems that linear deviation cannot be only attributed to entering a QTM regime but an additional process could be involved (Cole-Cole plots are not completely well reproduced with a single relaxation step model). This can be perturbing the thermal barriers parameters extracted only from the linear plot region.

In fact, we were able to nicely fit this data in the whole temperature range by including two thermal activated processes and a characteristic QT time (fig. S6):

$$\frac{1}{\tau} = \frac{1}{\tau_0^1}\exp\left(-\frac{U_{eff}^1}{kT}\right) + \frac{1}{\tau_0^2}\exp\left(-\frac{U_{eff}^2}{kT}\right) + \frac{1}{\tau_{QT}}$$

obtaining the following parameters: U^1_{eff}=102 K; τ^1_0= 1.8 x 10^{-8} s; U^2_{eff}=30K; τ^2_0= 1.2 x 10^{-4} s and τ_{QT}= 1.2 s. These thermal barriers compare well with complex **1** found ones, however this material contains two different Dy^{III} sites, hence this may also explain these two convoluted relaxation processes. Finally, for the complex $[Co^{III}_2Ln^{III}_2(OH)_2(bdea)_2(acac)_2(NO_3)_4]$, a U_{eff} value of 169K, the highest one among this series and one of the highest among all reported Dy_2 compounds, was reported. However, in this case again, linear deviation of the ln(τ) vs 1/T data plot profile cannot be reasonably reproduced by considering only a QTM pathway. We were able to fit these data in the whole temperature range by including an additional thermal activated pathway together with the QT mechanism. This affords: U^1_{eff}=147 K; τ^1_0= 5.0 x 10^{-7} s ; U^2_{eff}=61 K; τ^2_0= 5.6 x 10^{-5} s and τ_{QT}= 1.5 s. Under this new scenario, dynamic behaviour of this complex resembles our findings for complex **1** in the sense of possibly involving two pathways at zero DC. Nevertheless, this should be cautiously considered

as switching from an Orbach to a Raman type process may also be contributing in deviation from Arrhenius behaviour, hence affecting U_{eff} extracted values.

(1) G. Aromi, A. S. Batsanov, P. Christian, M. Helliwell, A. Parkin, S. Parsons, A. A. Smith, G. A. Timco, R. E. P. Winpenny, *Chem.-Eur. J.* **2003**, 9, 5142.

(2) SCALE3 ABSPACK: Empirical absorption correction, CrysAlis – Software package, Oxford Diffraction Ltd., Oxford, **2006**.

(3) G. M. Sheldrick, SHELXS97 and SHELXL97; Programs for Crystal Structure Resolution; University of Göttingen: Göttingen, Germany, **1997**.

Table ESI1. Crystallographic data of **1**.

Empirical Formula	C_{44} H_{86} Co_2 Dy_2 N_2 O_{20}
Formula weight	1406.01
T (K)	298 (2)
Crystal system	Triclinic
Space Group	P-1
a (Å)	10.9410 (4)
b (Å)	11.2485 (4)
c (Å)	12.2043 (5)
α (°)	104.787 (3)
β (°)	90.745 (3)
γ (°)	94.220 (3)
V (Å^3)	1447.50 (9)
Z	1
D_{calc} (mg/m^3)	1.613
Absorption coefficient (mm^{-1})	3.183
F(000)	710
Crystal size (mm)	0.12 x 0.40 x 0.51
Crystal color/shape	Blue blocks
Radiation, graphite monochr.	MoKα, λ = 0.71069 Å
θ Range data collection (°)	3.71 – 27.0
Index ranges	$-13 \leq h \leq 13$
	$-14 \leq k \leq 14$
	$-15 \leq l \leq 15$
Reflections collected/unique	18734/6252(Rint=0.0550)
Observed reflections [I>2σ(I)]	5086
Completeness (%)	99.1
Maximum / minimum transmission	1.000 / 0.544
Refinement method	full-matrix least-squares on F^2

Weights, *w*	$1/[\sigma^2(F_o^2)+(0.0423P)^2+1.4130P]$ where $P=(Fo^2+2F_c^2)/3$
Data/restraints/parameters	6252/30/314
Goodness-of-fit (GOF) on F^2	1.076
Final R-index [I>2σ(I)]/ all data	0.0384/ 0.0557
*w*R index [I>2σ(I)] /all data	0.0878/ 0.1011
Largest peak and hole (e A^{-3})	1.399 and -1.029

Table ESI2. Main bond angles (°) and distances (Å) of **1**.

Dy1-O12	2.360(4)
Dy1-O13	2.455(4)
Dy1-O14_a	2.253(3)
Dy1-O15_a	2.446(3)
Dy1-O15	2.454(3)
Dy1-O21	2.372(4)
Dy1-O23	2.388(4)
Dy1-O24	2.261(3)
Co2-N1	1.990(4)
Co2-O11	1.907(4)
Co2-O14	1.891(3)
Co2-O15	1.934(3)
Co2-O22_a	1.914(4)
Co2-O24	1.881(3)

Co2—O24—Dy1	105.03 (16)
Dy1_a—O15—Dy1	113.44 (13)
Co2—O15—Dy1	96.60 (14)
Co2—O15—Dy1_a	96.35 (13)
Co2—O14—Dy1_a	104.41 (14)
Co2_a—Dy1—Co2	102.95 (3)
Dy1_a—Co2—Dy1	77.05 (3)

Symmetry code: (a) 1-x, 2-y, 1-z

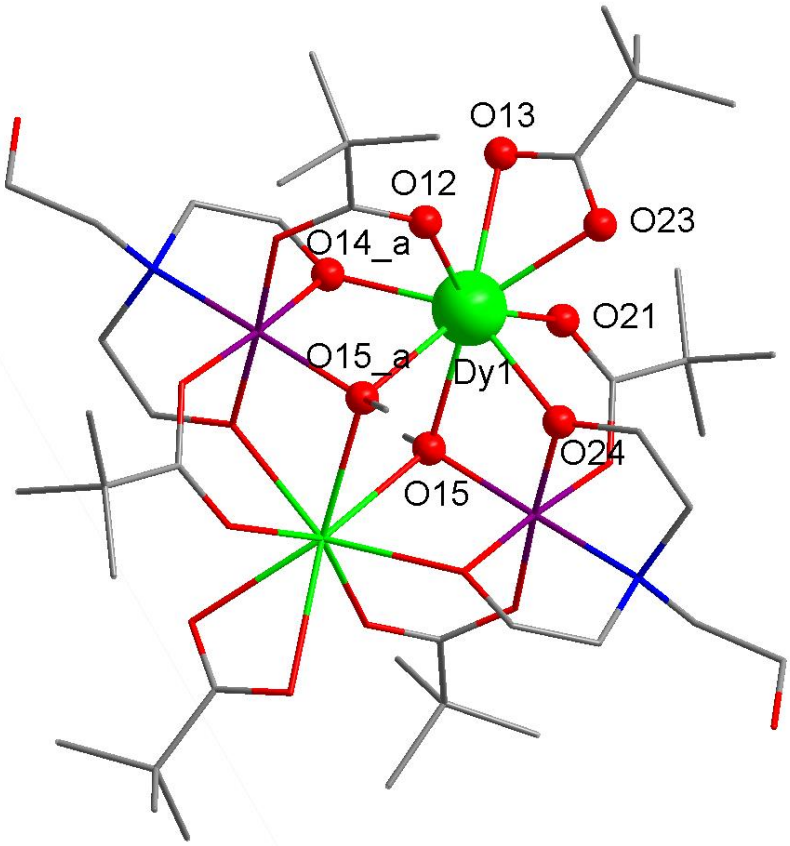

Figure ESI1. Molecular representation of complex **1** highlighting Dy^{III} ion coordination sphere. H atoms omitted for sake of clarity.

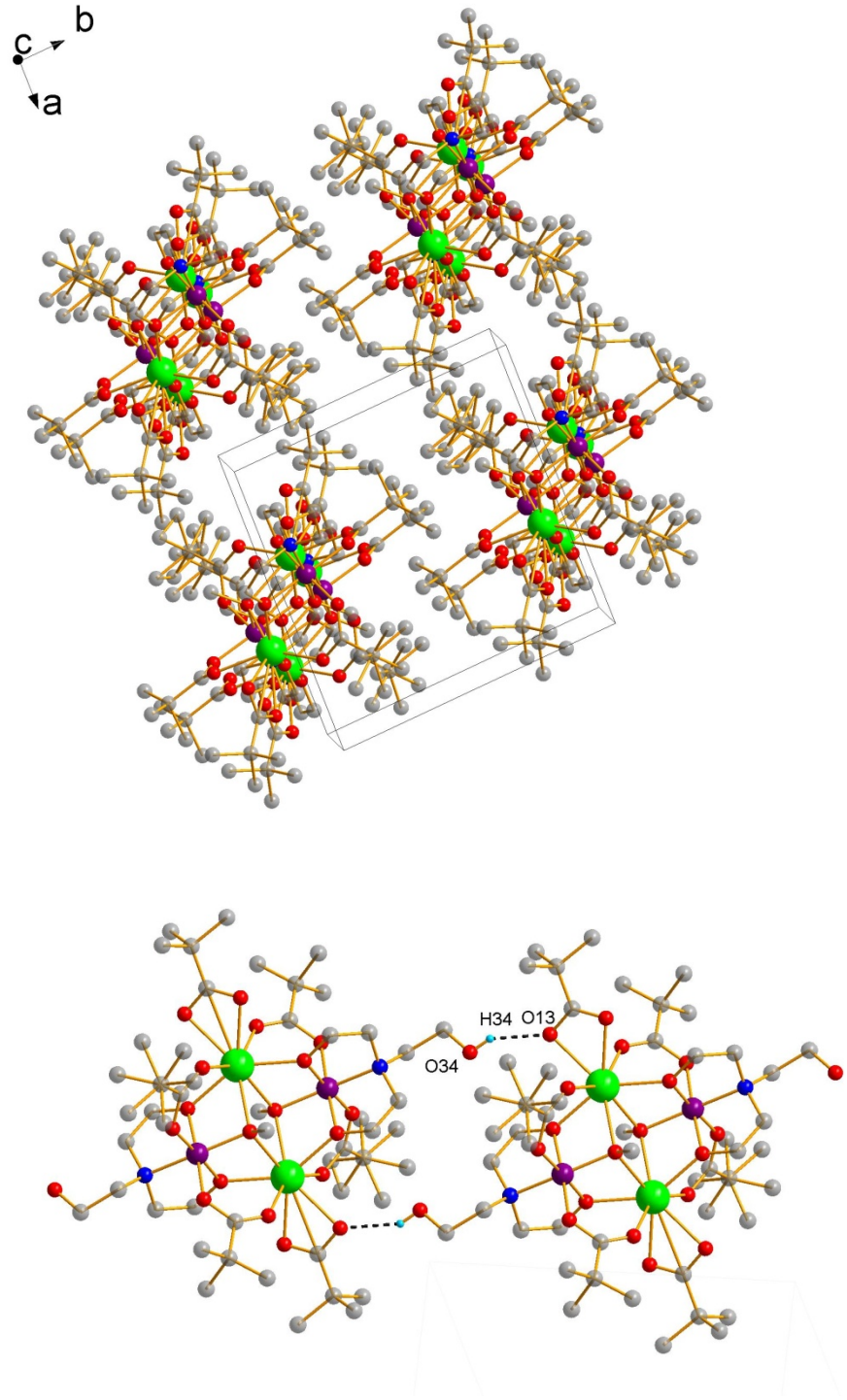

Figure ESI2. Top: Molecular representation of complex **1** crystal packing. View along *c*- axis. Bottom: Molecular representation of complex **1** highlighting the inter-molecular H-bond interactions. H atoms omitted for sake of clarity.

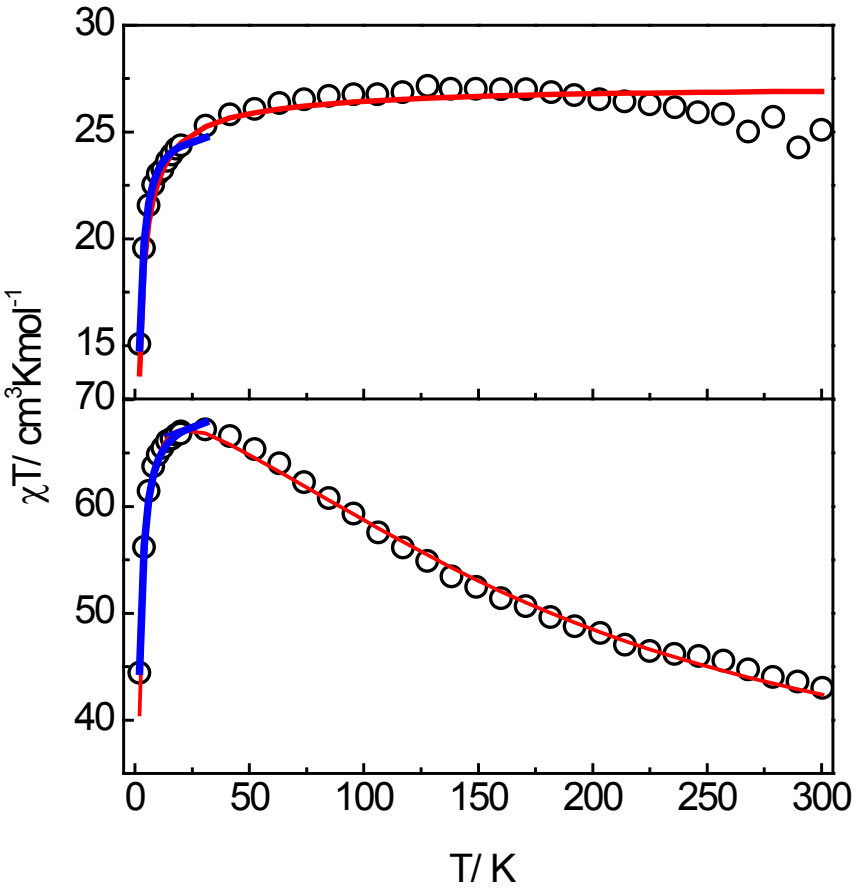

Figure ESI3. $\chi_m T$ vs T data plots (open circle) at 1 kOe between 2-300 K for complex **1**. Full line shows the simulated data with parameters described in the text (red line: full basis set; blue line: Ising exchanged S_{eff}=1/2 doublets). Top: silicone embedded sample; bottom: free sample.

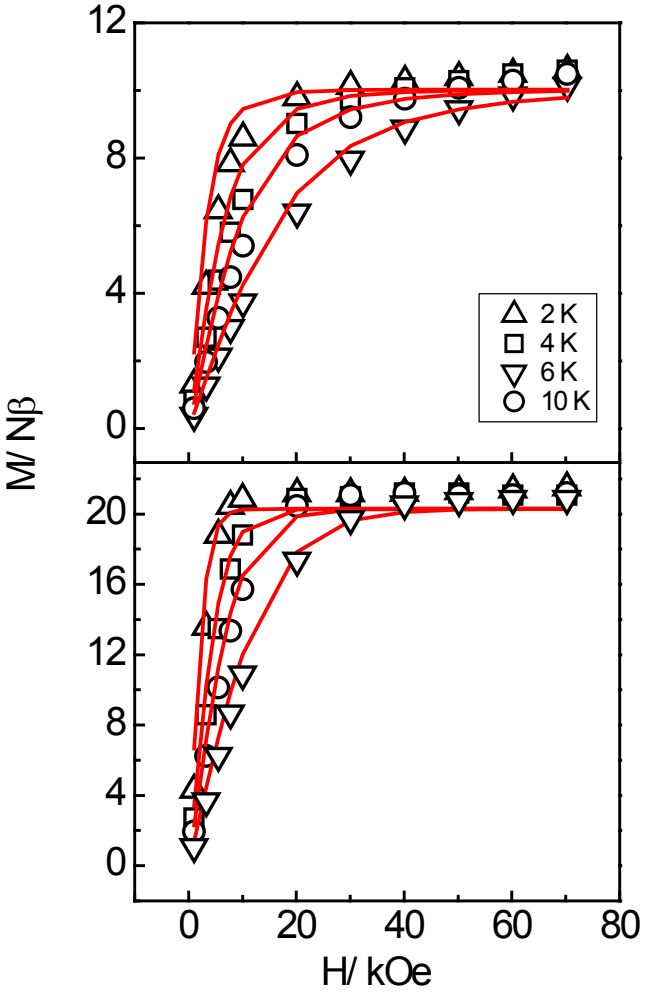

Figure ESI4. *M* vs *H* data plots (open symbols) at 2, 4, 6 and 10 K in the range 1-70 kOe for complex **1**. Full line shows the simulated data with parameters described in the text. Top: silicone embedded sample; bottom: free sample.

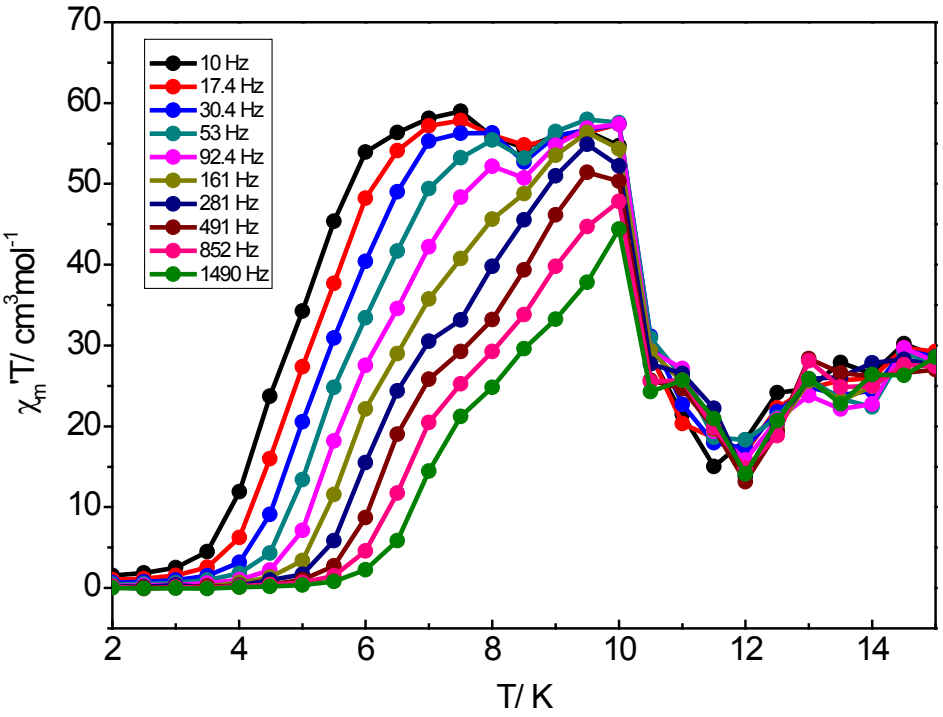

Figure ESI5. χ_m'T vs T data plot in the range 2-15 K, and driving frequencies between 10-1490 Hz for complex **1** at zero DC field.

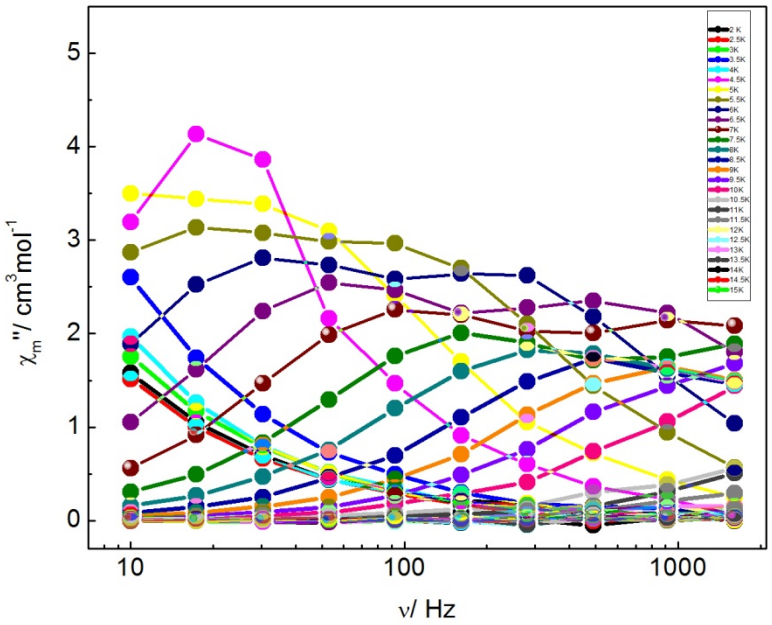

Figure ESI6. Frequency dependence of the out of-phase ac susceptibility, χ_m'', of **1** in a zero dc magnetic field. Frequency displayed in a logarithmic scale.

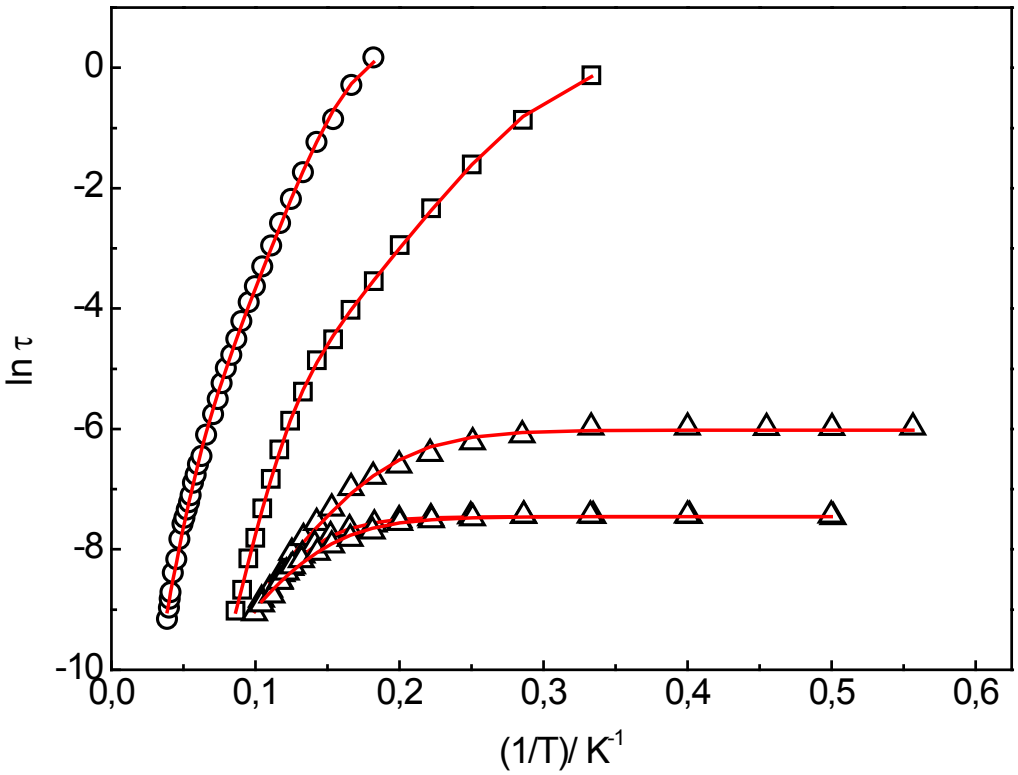

Figure ESI7. ln τ vs T^{-1} plots open symbols together with best fitting plots (full line) according to the different Arrhenius type expressions discussed in the text. Circles: $[Co^{III}_2Ln^{III}_2(OH)_2(bdea)_2(acac)_2(NO_3)_4]$ from Ref. 9 ; squares: $[Co^{III}_2Dy^{III}_2(OMe)_2(teaH)_2(O_2CPh)_4(MeOH)_2][NO_3]_2$. $[Co^{III}_2Dy^{III}_2(OMe)_2(teaH)_2(O_2CPh)_4(MeOH)_2(NO_3)_2]$ from Ref. 7 ; triangles: $[Co^{III}_2Dy^{III}_2(OR)_2(teaH)_2\ (acac)_4(NO_3)_2]$ from Ref. 8.

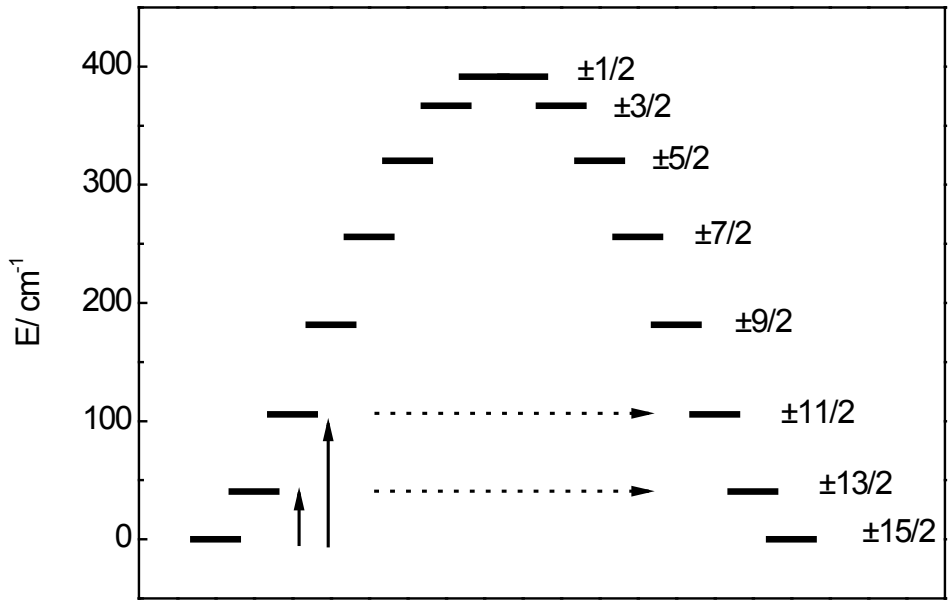

Figure ESI8. Energy level splitting under crystal field of the Dy^{III} ground J=15/2 state, with crystal field parameters, B_2^0=-2.4 cm^{-1} ; B_4^0= 2.9x10^{-3} cm^{-1}. Arrows indicate the suggested relaxation pathways across the barrier.

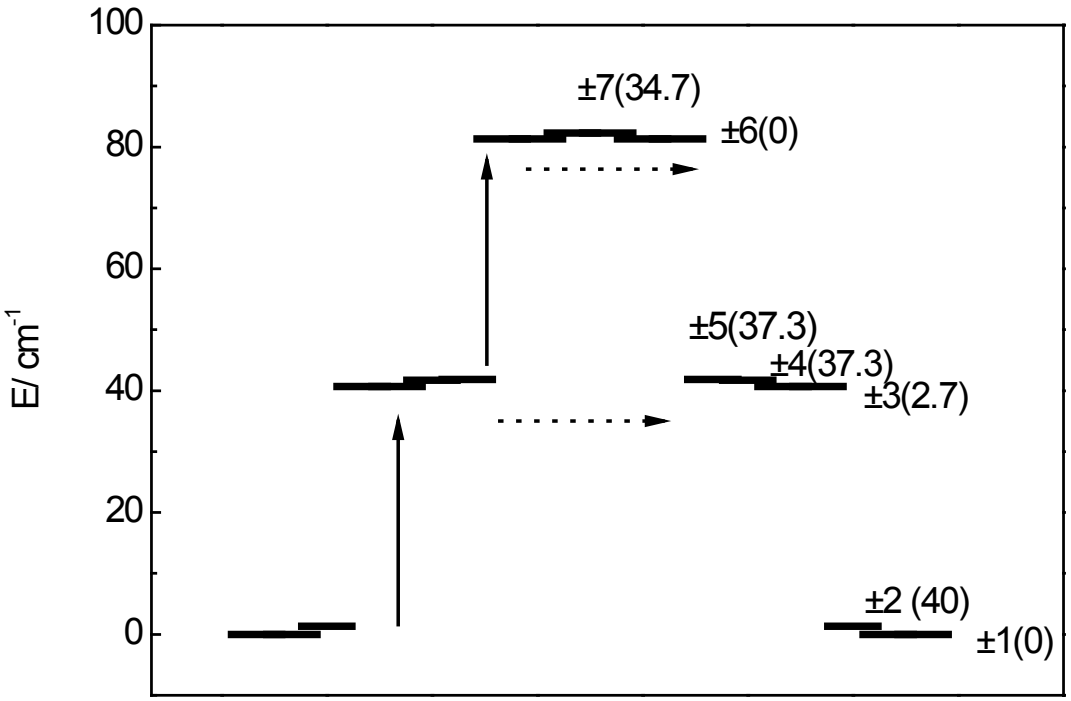

Figure ESI9. Energy level splitting under crystal field of both ground Dy^{III} J=15/2 exchange coupled states, with crystal field parameters, B_2^0 =-2.4 cm^{-1} ; B_4^0 = 2.9x10^{-3} cm^{-1} and exchange interaction J_{exc}=-0.046 cm^{-1}Arrows indicate the suggested relaxation pathways across the barrier. Doublets g_z^{eff} values between parentheses.